ELSEVIER

Contents lists available at ScienceDirect

Quaternary Science Reviews

journal homepage: www.elsevier.com/locate/quascirev





Aquatic moss $\delta^{18}O$ as a proxy for seasonally resolved lake water $\delta^{18}O$, northwest Greenland

Peter J.K. Puleo ^{a,*}, Pete D. Akers ^b, Ben G. Kopec ^c, Jeffrey M. Welker ^{d,e}, Hannah Bailey ^f, Magdalena R. Osburn ^a, Tenna Riis ^g, Yarrow Axford ^a

- ^a Department of Earth and Planetary Sciences, Northwestern University, Evanston, IL, USA
- ^b Discipline of Geography, School of Natural Sciences, Trinity College Dublin, Dublin, Ireland
- ^c Great Lakes Research Center, Michigan Technological University, Houghton, MI, USA
- ^d Ecology and Genetics Research Unit, University of Oulu, Finland
- e Department of Biological Sciences, University of Alaska Anchorage, Anchorage, Alaska, USA
- ^f Water, Energy and Environmental Engineering Research Unit, University of Oulu, Finland
- g Department of Biology, Arctic Research Center, Aarhus University, Aarhus C, Denmark

ARTICLE INFO

Handling editor: Mira Matthews

Keywords: Present Stable isotopes Aquatic moss Paleoclimatology Greenland Lakes and ponds Seasonality Water isotopes

ABSTRACT

Reconstructing past climate seasonality is fundamental to understanding the nature of past climate changes. This is especially true in the Arctic, where climate is intensely seasonal and proxies that can distinguish climate conditions of multiple seasons in a single year are relatively rare. We propose that submerged aquatic mosses, which are abundant subfossils in some Arctic lake sediments and have distinctive seasonal growth morphologies, can be used to estimate past lake water oxygen isotope composition $(\delta^{18}O_{lw})$ across multiple seasons. Aquatic mosses are abundant, well preserved, and grow continuously in Arctic lakes whenever light is available, with some species displaying unique seasonal morphologies influenced by water temperature. Although Greenland paleorecords suggest that aquatic moss oxygen isotope values ($\delta^{18}O_{om}$) reflect the $\delta^{18}O$ values of lake water, no modern calibration between $\delta^{18}O_{om}$ and $\delta^{18}O_{lw}$ exists in Greenland. We present a modern $\delta^{18}O_{om}$ vs. $\delta^{18}O_{lw}$ calibration using multiple moss species or morphotypes from eight lakes and ponds near Pituffik (Thule), northwest Greenland. We find strong linear relationships ($r^2=0.76$ -0.85) between the $\delta^{18}O_{om}$ and $\delta^{18}O_{lw}$ values of multiple species or morphotypes across the range of relatively low $\delta^{18}O_{lw}$ values at Pituffik, and our results indicate isotopic fractionations are similar to those found previously at lower latitudes. To assess the potential of mosses as archives of seasonal $\delta^{18}O_{lw}$ values, we analyzed $\delta^{18}O_{om}$ in season-specific segments of moss strands, with seasons identified based upon growth morphology. Moss inferred lake water δ^{18} O values (δ^{18} O_{lwom}) are higher in autumn than spring or summer, likely due to increasing contributions of ¹⁸O enriched precipitation and the cumulative effects of lake water evaporation throughout the ice-free season. For moss subsampled throughout summer, $\delta^{18}O_{lwom}$ values generally increased through the season in parallel with observed $\delta^{18}O_{lw}$ values. Potential temperature dependent fractionation effects during biosynthesis, however, remain unconstrained and should be further addressed with future research. Overall, these findings suggest that aquatic mosses from lake sediments could be used to directly resolve climate seasonality of the past.

1. Introduction

Reconstructing past temperature and precipitation seasonality is vital for improving our estimates of future glacier mass changes (Greene et al., 2024), agricultural production, and plant phenology (Collins et al., 2021). Climate seasonality is especially large in the Arctic, and although Greenland ice core proxies and other terrestrial

reconstructions provide critical records of Northern Hemisphere paleoclimate shifts, they do not typically reveal the seasonality of those climate changes and are often spatially limited (Denton et al., 2005; Buizert et al., 2018; Axford et al., 2021). Multiple periods of relatively recent abrupt climate change, like the Younger Dryas (12,900–11,700 cal yr BP [calibrated years before present, where present is 1950]) and "8.2 ka event," have been hypothesized to feature extreme shifts in

^{*} Corresponding author. 2145 Sheridan Road, Room F480, Evanston, IL, 60201, USA. *E-mail address:* peterpuleo2024@u.northwestern.edu (P.J.K. Puleo).

climate seasonality in Greenland (Alley, 2000; Alley and Ágústsdóttir, 2005; Denton et al., 2005; Puleo et al., 2022). Records from other parts of the Arctic suggest winter temperatures may have increased through the Middle to Late Holocene (Meyer et al., 2015; Holland et al., 2020) while summer temperatures decreased over the same period (Marcott et al., 2013) due to diverging seasonal insolation trends, but this has not been confirmed in Greenland. Reconstructing the seasonality of late Pleistocene and Holocene climate changes in the Arctic would facilitate understanding and modeling of how past climate changes affected ecosystems and the cryosphere, including the Greenland Ice Sheet, with implications for forecasting future sensitivity to anthropogenic warming.

Despite the importance of reconstructing air temperature across all seasons in the Arctic, most proxies are summer biased. Pollen assemblages archived in lake sediments are one exception and widely used to reconstruct summer, winter, and annual temperatures. However, pollen assemblage reconstructions can be subject to large uncertainties associated with long distance pollen transport, vegetation colonization lag times, and non-analog past ecosystems (Seppä et al., 2004; Fastovich et al., 2020). Winter temperatures may be particularly difficult to assess with pollen assemblage reconstructions in the Arctic due to their weaker relationship with pollen assemblages compared to summer temperatures (Fréchette et al., 2008). Pioneering work has used alkenones, when productivity is sufficient, to infer winter and spring temperatures (Longo et al., 2020; Richter et al., 2021), which can be compared with more common summer temperature reconstructions from pollen and chironomids. In addition, ice wedge δ^{18} O values are interpreted to largely reflect winter/spring temperatures as they form in cracks after permafrost thermally contracts in wintertime (Meyer et al., 2015; Holland et al., 2020). Overall, most terrestrial paleoclimate reconstructions that attempt to address seasonality have used multiple proxies that reflect different seasons (Meyer et al., 2015; Longo et al., 2020; Richter et al., 2021; Puleo et al., 2022). However, individual proxies are subject to various drivers and uncertainties, introducing additional uncertainties to seasonal comparisons when applied together.

Lake water δ^{18} O and δ^{2} H values in small, precipitation-fed, throughflowing lakes in Greenland and across the Arctic vary seasonally with changes in precipitation $\delta^{18}O$ and $\delta^{2}H$ values and climate (Allen et al., 2019), and act as tracers of these seasonal environmental shifts (Thomas et al., 2020; Corcoran et al., 2021; Akers et al., 2023; Harning et al., 2024). In northwest Greenland, major climate controls on the seasonal δ^{18} O and δ^{2} H values of water vapor include air temperatures and sea ice cover, with the latter having large effects on local moisture availability relating to local wind directions and synoptic storm tracks (Akers et al., 2020). In lakes strongly affected by evaporation, lake water δ^{18} O and δ²H values will also reflect cumulative evaporative enrichment in ¹⁸O and ²H throughout the ice-free season. The oxygen isotope values of bulk aquatic moss tissues ($\delta^{18}O_{om}$) have been shown to primarily reflect lake water oxygen isotope values ($\delta^{18}O_{lw}$) since they incorporate growth water into cellulose and other organic compounds (Zhu et al., 2014) and have been utilized in multiple paleoclimate reconstructions from Greenland (Lasher et al., 2017; Puleo et al., 2022). This is a powerful proxy as aquatic mosses are common, well-preserved in lake sediments, and easy to prepare for analysis due to the small sample mass required for $\delta^{18}O$ measurement. Additionally, using aquatic mosses for $\delta^{18}O$ measurements eliminates terrestrial vs. aquatic source attribution uncertainty associated with sediment cellulose extractions, and these submerged mosses are not affected by evapotranspiration-induced isotopic effects (Sauer et al., 2001; Zhu et al., 2014). However, aquatic mosses are composed of multiple chemical components including cellulose, polyphenols, fats, oils, waxes, and carbohydrates, and each component likely has its own $\delta^{18}O$ fractionation offsets from $\delta^{18}O_{lw}$ values. Therefore, $\delta^{18}O_{om}$ measurements require calibrations with $\delta^{18}O_{lw}$ values separate from cellulose $\delta^{18}O$ values, which are already well calibrated with $\delta^{18}O_{lw}$ values across a range of plant types and locations (DeNiro and Epstein, 1981; Sauer et al., 2001; Mayr et al.,

2015). Thus far, $\delta^{18}O_{om}$ to $\delta^{18}O_{lw}$ calibration studies are geographically limited to Patagonia and cover only a few aquatic moss species (Zhu et al., 2014).

With further calibration, $\delta^{18}O_{om}$ values could be used as a single proxy to quantitatively estimate past climate seasonality in the Arctic. These mosses are abundant in polar regions as they can tolerate relatively low light and nutrient poor environments (Riis and Sand-Jensen, 1997; Riis et al., 2010; Rankin et al., 2017; Thiemer et al., 2018). This means they grow and record $\delta^{18}O_{lw}$ values through multiple seasons. Studies have shown that several species of Arctic and Antarctic aquatic brown mosses of the family Amblystegiaceae exhibit seasonal changes in growth morphology that make it possible to identify the season of growth along individual moss strands (Riis and Sand-Jensen, 1997; Li et al., 2009; Guo et al., 2013; Riis et al., 2014; Thiemer et al., 2018; Xia et al., 2020). Thus, in lakes with seasonal variations in $\delta^{18}O_{lw}$, mosses could be split into seasonally specific samples based on morphology and used for reconstructing seasonally specific $\delta^{18}O_{lw}$ values.

To advance understanding of this potential seasonal proxy, we address the following research objectives:

- 1) Establish a modern $\delta^{18}O_{om}$ to $\delta^{18}O_{lw}$ calibration using modern field samples of several aquatic brown moss species/morphotypes from eight pond and lake sites (hereby referred to as lakes) near Pituffik, northwest Greenland.
- 2) Determine if subsampling and measuring the $\delta^{18}O$ values of morphologically distinct, seasonal growth strands of aquatic mosses reflects the evolution of $\delta^{18}O_{lw}$ values within and across multiple seasons.

2. Site description

The Pituffik (Thule) region of northwest Greenland is an ideal location to develop an $\delta^{18}O_{om}$ vs. $\delta^{18}O_{lw}$ calibration and to test a potential novel seasonality proxy as it has numerous lakes, extensive aquatic moss growth, systematic modern water isotope sampling (Akers et al., 2023), and large modern climate seasonality (Cappelen and Drost Jensen, 2021). Some $\delta^{18} O_{om}$ measurements on moss samples collected from lake sediment cores have been used to infer paleoclimate change alongside other more well established $\delta^{18}O$ proxies (Lasher et al., 2017; Puleo et al., 2022), however, $\delta^{18}O_{lw}$ was estimated using a calibration model based on data collected in Patagonia as a calibration dataset from Greenland does not currently exist. Additionally, those studies did not attempt to identify the season of growth of the moss strands used for $\delta^{18}O_{om}$ analyses. To develop the first $\delta^{18}O_{om}$ vs. $\delta^{18}O_{lw}$ calibration in Greenland and to evaluate a potential novel seasonality proxy, we selected eight sites north and northeast of Pituffik Space Base (Table 1; Fig. 1) to sample for aquatic mosses.

Annual average temperature from 1991 to 2020 CE in Pituffik is -10.2 °C, with a mean January temperature of -23.9 °C and a mean July temperature of 6.1 °C (Fig. 2B; Cappelen and Drost Jensen, 2021). The annual precipitation amount is 149.4 mm, and the majority falls in July, August, September, and October (Fig. 2C; Cappelen and Drost Jensen, 2021). Satellite imagery, field observations (Akers et al., 2023), and climate data (Cappelen and Drost Jensen, 2021) suggest the study lakes are ice-free or at least have ice-free moats from early/mid-June to late August/early September. The exact timing varies annually among sites depending on weather conditions (Akers et al., 2023). Bedrock around the sites is late Precambrian dolomite and a gneiss-schist-granite complex (Dawes et al., 1973; Dawes, 1975). The Pituffik region is covered by glacial deposits (Corbett et al., 2015) with sparse tundra dominated by Carex, Dryas, and dwarf Salix. The lakes formed in the Late Pleistocene following glacial retreat (Corbett et al., 2015). Thick moss mats cover the nearshore or entire bottoms of many lakes and ponds near Pituffik, and subfossil remains of Amblystegiaceae are abundant in Holocene and Last Interglacial lake sediments from the region (Lasher et al., 2017; McFarlin et al., 2018, 2023).

Table 1
Locations, elevations, surface area, water depth (NA if not available), and hydrologic category for our eight sites. For Hydrology, DS = Downstream, HW = Headwater, and ER = Endorheic (Akers et al., 2023).

Site	Latitude (°N)	Longitude (°W)	Elevation (m a.s.l.)	Surface Area (m ²)	Max Water Depth (m)	Hydrology
Diabase Depth Lake (DBL)	76.5710°	−68.6847°	195	21,365	NA	DS
Lioness Rock Lake (LEO)	76.5683°	-68.6887°	170	10,835	1.3	ER
North Mountain View Lake (NML)	76.5671°	−68.6699°	80	7610	NA	DS
Lake Potato (PL)	76.5569°	-68.5481°	185	59,960	NA	DS
Power Lake (PWL)	76.5462°	-68.5516°	180	60,460	NA	HW
Shaley Point Lake (SPL)	76.5731°	-68.6930°	205	22,070	NA	HW
Upper Lake Potato (UPL)	76.5607°	-68.5662°	195	51,040	NA	DS
Water Garden Lake (WGL)	76.5674°	-68.4423°	45	21,340	1.54	ER

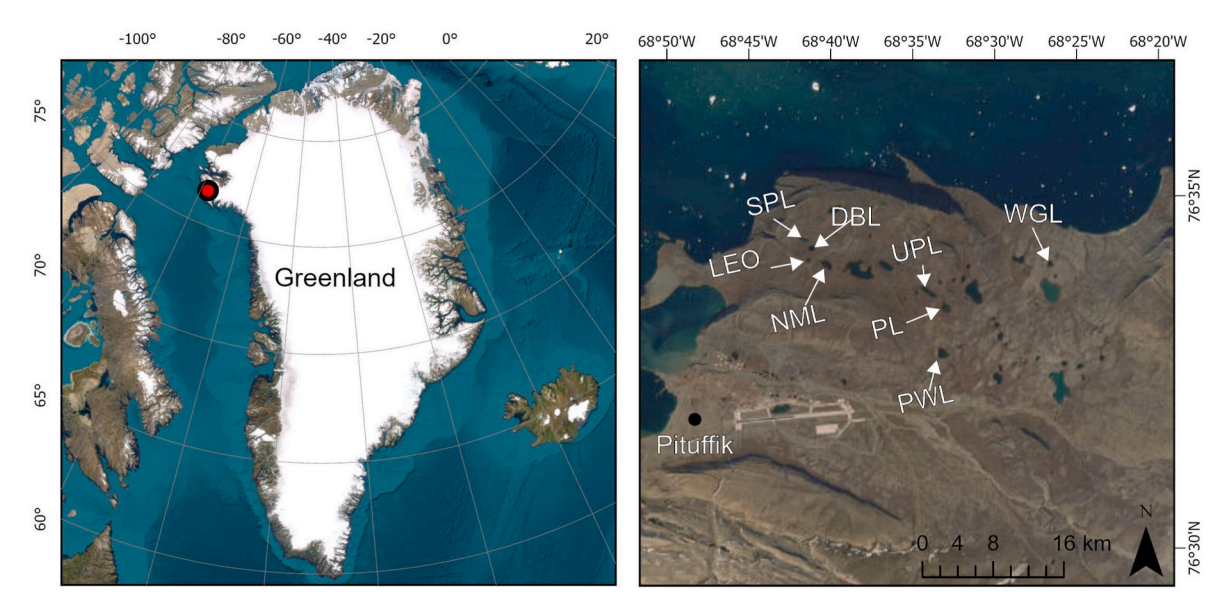


Fig. 1. A) A map of Greenland. The red and black symbol indicates the study area near Pituffik, northwest Greenland. B) The study area around Pituffik and the Pituffik Space Base (formerly Thule Air Base) with abbreviated site names (see Table 1 for full names). Made using ESRI ArcGIS Pro and Earthstar Geographics.

All eight sites are precipitation fed with a large spring (May/June) snowmelt input and minimal inputs of groundwater due to continuous permafrost and a thin active layer. Additionally, none of the sites have glaciers, large permanent snowfields within their watersheds, or receive meltwater input from the Greenland Ice Sheet (Akers et al., 2023). We have assigned each lake to one of several hydrological categories (Table 1): A headwater lake is the uppermost lake in a watershed, and has no inputs from other lakes, whereas a downstream lake receives upstream water from at least one other lake. Both of these categories are used for through-flowing lakes with active outflows in late summer. Lake interconnections may be through streams or shallow subsurface flow, and the interconnections are often dry or frozen for 7–8 months of the year (Akers et al., 2023). Endorheic lakes are found in small, hydrologically closed basins with no clear inflow or outflow channels.

3. Materials and methods

3.1. Pituffik field sampling

Lake water samples and aquatic moss samples at the sediment-water interface were collected from the eight sites near Pituffik in northwest Greenland in the summer of 2022. Water samples were stored in 20 mL Nalgene bottles, and aquatic mosses obtained from fully submerged, shallow-water (0.5–2 m depth) sites on lake bottoms were gently squeezed to remove excess water and stored in 50 mL plastic centrifuge tubes, Teflon bags, or Whirl-Pak bags. Moss and water samples were stored in a dark refrigerator at 4 °C until analysis. Mosses were not identified to the genus/species level, but two distinct morphotypes

(which we designate Species/Morphotype A and Species/Morphotype B) were separated (Supplementary Fig. 1). We assign the mosses in our study to the brown moss family Amblystegiaceae, and likely the genera *Drepanocladus, Warnstorfia*, and/or *Scorpidium*, which have been documented in modern surveys and Quaternary sediments near Thule/Pituffik (Steere, 1975; Hedenäs and Bennike, 2003) and are widely abundant and ecologically important in Arctic lakes (Steere, 1939; Riis et al., 2010; Guo et al., 2013; Riis et al., 2014). For two sites (LEO, WGL) in 2022, water samples were taken at separate times in summer. Our 2022 water samples were combined with previous isotopic sampling of the eight sites in summers 2018 and 2019 that was continuous and at a higher resolution across the ice-free season (Akers et al., 2023) for a total of 50 water isotope samples with a minimum of three separate sampling times per site.

3.2. Lake watershed and residence time calculations

We modeled watershed areas for LEO and WGL since they were the only sites with lake depth measurements that could be used to tentatively estimate lake volume and therefore residence time. We note that these are especially small lakes (ponds) from among those in our study; their small size meant they were ice-free earlier than others, and could be navigated by boat in late June/early July 2022 to measure their maximum depths. We demarcated watersheds with the ESRI ArcGIS Pro Hydrology toolset and a 2 m resolution ArcticDEM (Porter et al., 2018). Residence time was estimated using the following equation:

$$R = V / Q$$
 Eq. 1

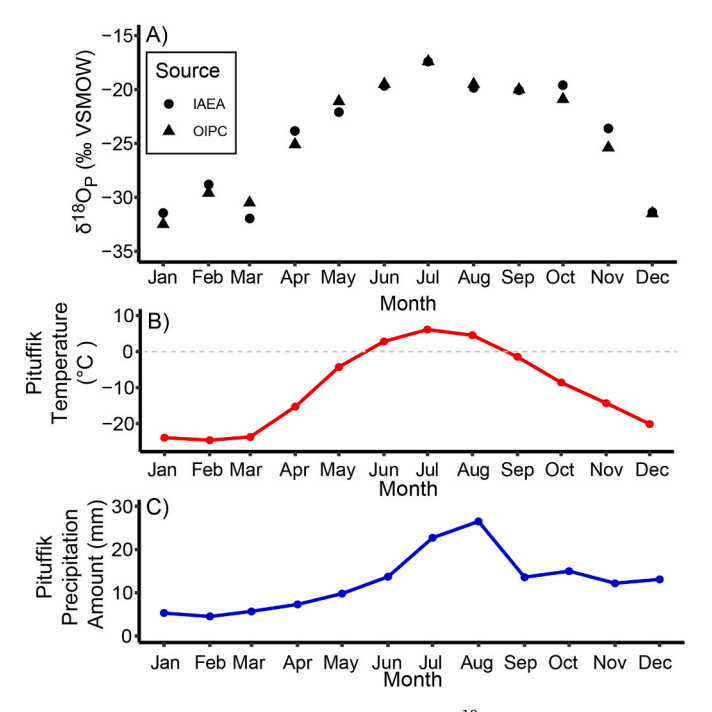


Fig. 2. A) Monthly average Pituffik precipitation δ^{18} O values measured from 1966 to 1971 (IAEA/WMO, 2015) and modeled for 2023 (OIPC; Bowen et al., 2005; Bowen, 2023). B) Monthly mean temperature data from Pituffik (1991–2020) near the study sites (Cappelen and Drost Jensen, 2021). C) Monthly mean precipitation amount data from Pituffik (1991–2020) near the study sites (Cappelen and Drost Jensen, 2021).

where R is the residence time in years, V is the lake volume (estimated using the product of the average depth of the lake and the surface area of the lake determined in Google Earth Pro), and Q is the annual inflow (estimated using the product of annual precipitation input (1991–2020 average; Cappelen and Drost Jensen, 2021) and the estimated watershed area). These approximate residence time estimates assume that lakes are of uniform depth, there is no net change in lake volume over the years, the volume of evaporative loss is minimal, and there is no long-term precipitation infiltration into or groundwater movement from the watersheds' mostly frozen ground.

3.3. δ^{18} O and δ^{2} H measurements

 $\delta^2 H$ and $\delta^{18} O$ values of 2022 lake water were measured on a Picarro Water Isotope Analyzer (model L2130-I with micro-combustion module A0325), in 8 or 9-fold replicates. Reported lake water $\delta^{18} O$ and $\delta^2 H$ values are the average of the last 5 replicates in the measurement series. They were corrected to known standards and calibrated to the VSMOW scale. Water samples from 2018 to 2019 were analyzed and corrected as described in Akers et al., 2023). Analytical uncertainty is $\pm 0.1\%$ for $\delta^{18} O$ and $\pm 0.6\%$ for $\delta^2 H$.

Aquatic mosses were thoroughly cleaned with DI water on a 250 μm sieve and viewed under a dissecting microscope to ensure cleanliness. No chemical pretreatment was utilized, as it was deemed unnecessary and could alter the isotopic composition of organic matter (Verbruggen et al., 2010). Strands were photographed to preserve morphological information. Cleaned, freeze-dried moss samples were cut into small pieces and placed in silver capsules, then analyzed for $\delta^{18}O$ values on a Thermo TC/EA, held at 1420 °C, coupled with Thermo Delta V + IRMS via a Conflo IV interface. The TC/EA was equipped with a 1.5 m long molecular sieve 5 Å GC column to provide for separation and prevent co-elution of N_2 and analyte CO. Isotope standards used for analysis consisted of BaSO4 standards (NBS127, IAEA-SO5, and IAEA-SO6), USGS water standards (GISP, VSMOW, and UCO3), and an in-house

cellulose standard. The analytical precision of the $\delta^{18}O_{om}$ values is $\pm 0.4\%$ and values are reported on the VSMOW scale. Isotope measurements are expressed as δ values in units of per mil (‰), where $\delta=(R_{sample}/R_{standard}-1)*1000$ and R is the ratio of $^{18}O/^{16}O$ of samples or standards.

For each site, 2-4 moss strands were selected for the calibration of $\delta^{18}O_{om}$ values to $\delta^{18}O_{lw}$ values. Each strand was used for a separate δ18O_{om} measurement. These strands had densely arranged leaves and were interpreted to reflect summer-season growth (Li et al., 2009; Guo et al., 2013), thus corresponding with our summer lake water isotopic measurements. A total of 28 moss samples were measured across the 8 sites for calibration. Sample mass ranged from 0.36 to 0.44 mg. Regression lines specific to species/morphotype (Species/Morphotype A and Species/Morphotype B; see Supplemental Fig. 1) and also to all species combined were calculated using the 2-4 aquatic moss warm (summer) season calibration samples per site (when present) and a site-based average of all summer lake water isotope measurements from each site. The fractionation factor between $\delta^{18}O_{om}$ values and $\delta^{18}O_{lw}$ values ($\alpha_{om\text{-lw}}$) were calculated as follows: ($\delta^{18}O_{om}$ / 1000+1) / ($\delta^{18}O_{lw}$ / 1000 + 1). These calibrations allow for inferring $\delta^{18}O_{lw}$ values from $\delta^{18}O_{om}$ measurements ($\delta^{18}O_{lwom}$).

To determine if mosses record seasonal and sub-seasonal changes in $\delta^{18}O_{\text{lw}}$ values, we conducted two sampling schemes. Our first sampling scheme assessed changes in $\delta^{18}O_{om}$ (and by using our calibration, $\delta^{18}O_{lwom}$) within a single summer's growth in individual moss strands. A single warm season (summer) aquatic moss sample at each site was selected to be split into 3-5 subsamples (i.e. sections, depending on available sample mass) for δ^{18} O measurement. Warm season growth was identified based on longer and more densely arranged leaves and branches, yielding a "bushy" morphology compared with "stringy" colder-season growth (Fig. 3; Riis and Sand-Jensen, 1997; Li et al., 2009; Guo et al., 2013; Riis et al., 2014; Thiemer et al., 2018; Xia et al., 2020). A total of 34 warm season (summer) samples were measured across the 8 sites, with 3-5 consecutive samples at each site depending on sample mass. The sampled summer for each moss strand was not necessarily 2021, as moss segments were selected for clear seasonal morphology rather than known age. Sample mass of the moss sections ranged from 0.12 to 0.43 mg.

Our second sampling scheme compares $\delta^{18}O_{om}$ for warm- (summer) vs. cooler-season (spring/fall) aquatic moss growth. Three strands with clear changes in seasonal growth morphology were selected from each lake site. Note that not all aquatic moss individuals had clear seasonal variations, possibly due to species variations or due to rapid, complex communal growth in thick moss mats that cause moss strands to get buried and minimize growth below the surface (Riis et al., 2010). The selected, seasonally varying mosses were each split into two (summer vs. spring or fall) subsamples based on morphologies (Fig. 3; Riis and Sand-Jensen, 1997; Li et al., 2009; Guo et al., 2013; Riis et al., 2014; Thiemer et al., 2018; Xia et al., 2020). Summer sections were identified as described above, while "stringy" sections with shorter/more sparsely arranged leaves are an indicator of growth under the colder conditions of some portion of spring and fall, when adequate light is available at the lake bottoms, but air and water temperatures are cold. Although they can grow under low light levels, aquatic mosses are light-dependent and would not grow in the winter due to complete darkness of polar winter and the thick layers of snow-covered ice at our high latitude sites (Riis et al., 2010). We rule out that sparser leaf coverage could be attributable to grazing or decomposition given how well our sample morphologies resemble documented season-specific growth morphologies in similar Arctic mosses, the relative lack of grazers in Arctic settings, and the lack of any obvious decomposition in these fresh, modern samples. Temperature is likely a driving factor in the changing seasonal growth morphologies of the species at our sites as has been suggested elsewhere in the Arctic (Riis and Sand-Jensen, 1997; Sand-Jensen et al., 1999; Guo et al., 2013; Riis et al., 2014; Manolaki et al., 2022). Differentiating spring cold-season from fall cold-season growth is possible based on

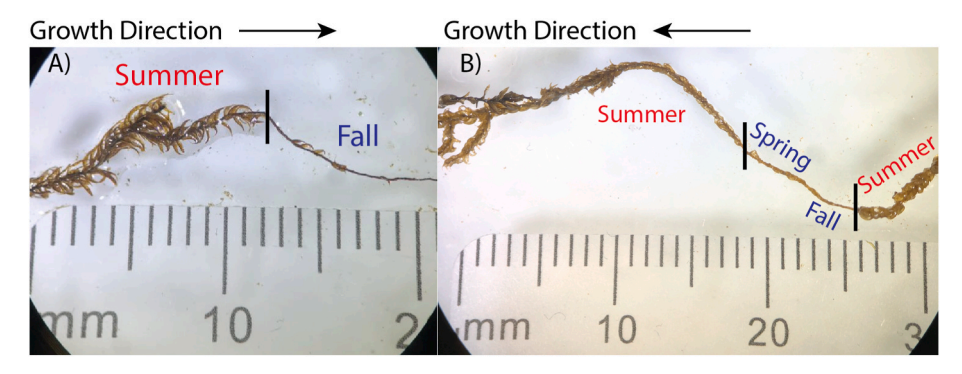


Fig. 3. Example morphologies of A) a two-season moss strand and B) a four-season moss strand from this study. "Bushy" sections with densely arranged leaves and branches reflect warm (summer) season growth while "stringy" sections with very few leaves and branches reflect cold (fall/spring) season growth (Li et al., 2009; Guo et al., 2013). The vertical black line shows where the mosses were split into seasonal samples prior to δ^{18} O measurement. The growth direction is indicated by the direction of the leaves, allowing us to identify spring growth (just before summer) and fall growth (just after summer).

growth direction of the moss strands, which can be inferred from the axil (Fig. 3). We note it is possible that the cold season (spring or fall) samples could contain a mixture of growth during the spring and fall seasons as they would grow back-to-back given the absence of light during the polar winter at our sites (no winter season growth), but we tried to avoid this by sampling immediately before/after the seasonal morphological transition. In total, 24 pairs of warm and cold season subsamples were analyzed, and sample mass ranged from 0.11 to 0.44 mg.

4. Results

4.1. Lake watershed and residence time estimates

Watershed area and residence time estimates were only calculated for WGL and LEO as they were the only two sites with water depth measurements. We estimated average depths of 1.1 \pm 0.2 m for WGL and 0.9 \pm 0.2 m for LEO. WGL has a watershed area of 80,475 m² and LEO has a watershed area of 31,505 m². Lake volume estimates range from 19,205–27,745 m³ for WGL and 7585–11,920 m³ for LEO. Average annual precipitation input was 0.132 m at Pituffik between 1991 and 2020 (Cappelen and Drost Jensen, 2021). The calculated inflow (Q) is 10,625 m³/yr for WGL and 4160 m³/yr for LEO. Using Eq. (1), WGL has an estimated water residence time of 2.2 \pm 0.4 years and LEO has an estimated water residence time of 2.3 \pm 0.5 years. The reported

uncertainty is from the range of lake volume estimates made using minimum and maximum estimated average lake depths. Again, these are tentative values given the range of uncertainty associated with the lake volume estimates.

4.2. Precipitation δ^{18} O values vs. lake water δ^{18} O values

Annual precipitation $\delta^{18}{\rm O}$ values from the Thule Air Base (76.52°N, $-68.83^{\circ}{\rm W}$) between 1966 and 1971 ranged from -31.5% to -17.4% (Fig. 2A; IAEA/WMO, 2015). Modern values estimated at the same latitude, longitude, and elevation as the IAEA/WMO station using the Online Isotopes in Precipitation (OIPC) calculator ranged from -32.5% to -17.4% (Fig. 2A; Bowen et al., 2005; Bowen, 2023). JJA precipitation $\delta^{18}{\rm O}$ values ranged from -19.9% to -17.4% (IAEA/WMO) and -19.5% to -17.4% (OIPC). The modern annual weighted average precipitation $\delta^{18}{\rm O}$ value calculated using monthly precipitation amount data (Cappelen and Drost Jensen, 2021) and precipitation oxygen isotope data from the OIPC (Bowen et al., 2005; Bowen, 2023) was -22.5%.

 $\delta^{18}O_{lw}$ values from our eight sites in 2022 (June–August) ranged from -21.3% to -8.4% (Fig. 4C). Including the 2018 and 2019 (June–August) water isotope data from these eight sites (Akers et al., 2023) slightly increased the range to -22.6% to -8.4% (Fig. 4A–C). By site, the combined averages of the 2018, 2019, and 2022 $\delta^{18}O_{lw}$ values were: DBL $=-18.7\pm1.2\%$ (n =4), LEO $=-13.0\pm1.0\%$ (n =4), NML

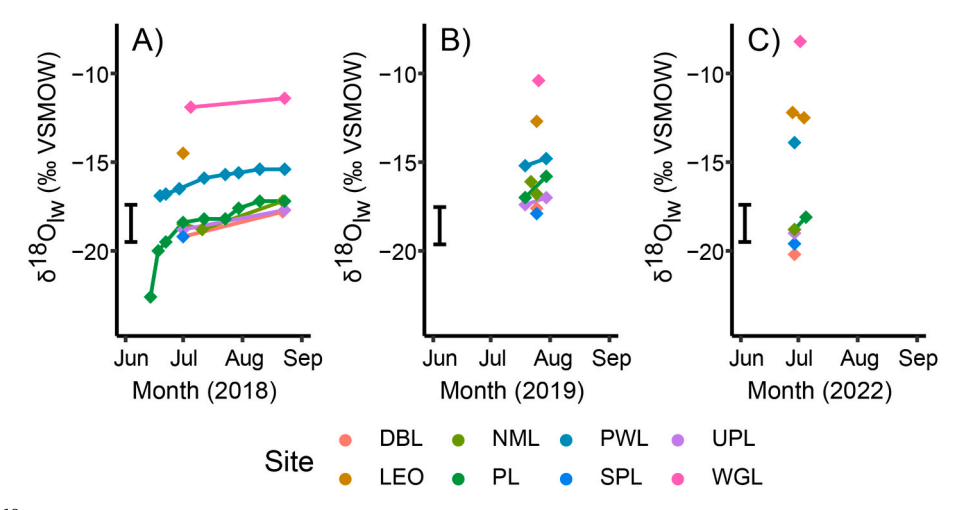


Fig. 4. A) Site specific $\delta^{18}O_{lw}$ values from 2018 lake water measurements near Pituffik (Akers et al., 2023). Black symbol indicates the range of mean JJA precipitation $\delta^{18}O$ values ($\delta^{18}O_p$) at Pituffik (1966-1971; IAEA/WMO, 2015). B) Site specific $\delta^{18}O_{lw}$ values from 2019 lake water measurements near Pituffik (Akers et al., 2023). C) Site specific $\delta^{18}O_{lw}$ values from 2022 lake water measurements near Pituffik (this study). Analytical uncertainty of any given $\delta^{18}O_{lw}$ measurement is less than the symbol size.

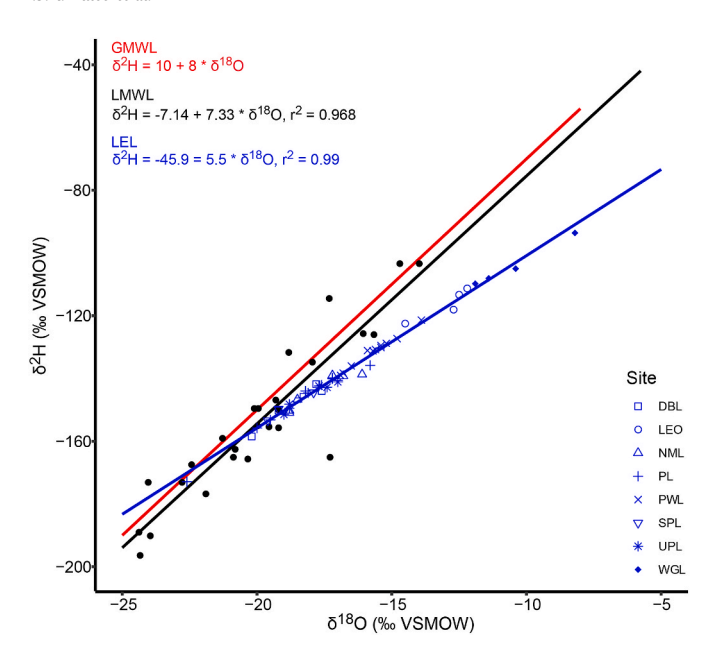


Fig. 5. A Global meteoric water line (GMWL; red line), local meteoric water line (LMWL; black line and points; developed using monthly data from 1966 to 1971 (IAEA/WMO, 2015)), and a local evaporative line (LEL; blue line and points; developed using 2018, 2019, and 2022 lake water data from Akers et al., 2023 and this study).

 $=-18.0\pm0.9\%$ (n =6), PL $=-18.0\pm1.1\%$ (n =13), PWL $=-15.7\pm0.9\%$ (n =11), SPL $=-18.9\pm0.9\%$ (n =3), UPL $=-18.0\pm0.9\%$ (n =5), and WGL $=-10.5\pm1.6\%$ (n =4). We found spring (mid to late June) $\delta^{18}O_{lw}$ values were lowest, summer (early July to mid-August) $\delta^{18}O_{lw}$ values were in the middle, and fall (late August to early September) $\delta^{18}O_{lw}$ values were the highest (Fig. 4A–C).

Using the $\delta^{18}O$ and $\delta^{2}H$ values of lake water from 2018, 2019, and 2022, we developed a local evaporation line to compare with the local meteoric water line made using the 1966–1971 precipitation $\delta^{18}O$ and $\delta^{2}H$ data (IAEA/WMO, 2015; Fig. 5). We find that the endorheic ponds WGL and LEO fall furthest out on the local evaporation line (Fig. 5), reflecting their greater evaporative modification. The amount of lake water evaporation each year can vary greatly depending on weather conditions (Akers et al., 2023).

4.3. Comparing aquatic moss δ^{18} O with lake water δ^{18} O values

Summer $\delta^{18}O_{om}$ values and site-averaged summer $\delta^{18}O_{lw}$ values are strongly linearly correlated regardless of species/morphotype and whether or not the strand $\delta^{18}O_{om}$ values are averaged by site. $\delta^{18}O_{om}$ values across all eight sites ranged from 8.1% to 14.6% in the summer calibration samples (n = 28) while the site-averaged summer $\delta^{18}O_{lw}$ values ranged from -18.9 to -10.5% (n = 50). The all-species linear regression for individual strand $\delta^{18}O_{om}$ values (Fig. 6) is given as:

$$\delta^{18}O_{om}\!=\!0.635(\pm0.07)*\delta^{18}O_{lw}\!+\!21.24(\pm1.20); r^2\!=\!0.755; n\!=\!28 \hspace{0.5cm} \text{Eq.} 2$$

where $\delta^{18}O_{lw}$ is the $\delta^{18}O$ value of average lake water and $\delta^{18}O_{om}$ is the $\delta^{18}O$ value of individual aquatic moss strands. The fractionation factor between $\delta^{18}O_{om}$ values and $\delta^{18}O_{lw}$ values $(\alpha_{om\cdot lw})$ for the all-species linear regression samples is 1.0278 \pm 0.0014‰. Utilizing a species-based average of $\delta^{18}O_{om}$ values for each species/morphotype by site (Fig. 6), rather than plotting all individual $\delta^{18}O_{om}$ samples, yielded the following equation:

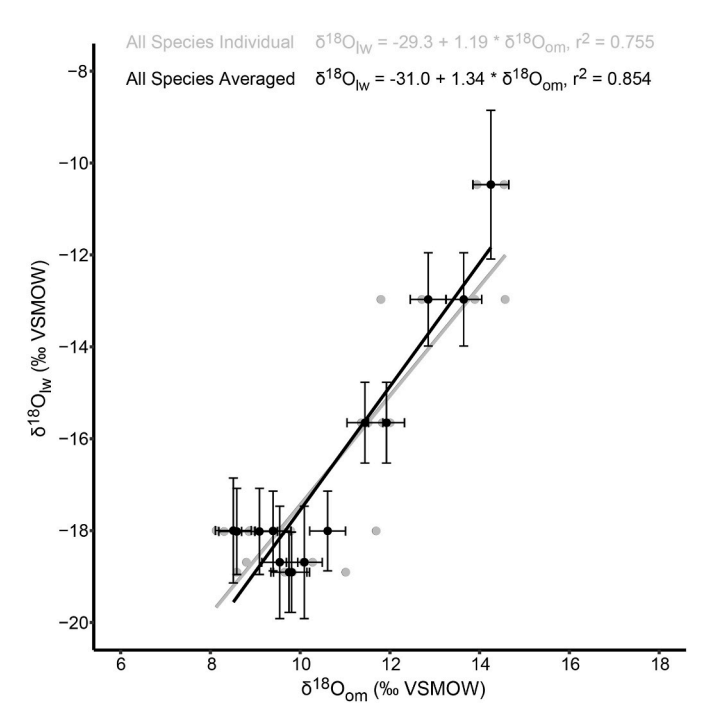


Fig. 6. Summer aquatic moss $\delta^{18}O$ ($\delta^{18}O_{om}$) values vs. summer lake water $\delta^{18}O$ ($\delta^{18}O_{lw}$) values for all species/morphotypes of moss and all sites in this study. Note that the independent and dependent variables are swapped compared to Eq. 2 and Eq. 3 (to infer $\delta^{18}O_{lw}$ values from $\delta^{18}O_{om}$ values). Raw individual strand values with two samples per species/morphotype at each site are shown as gray dots (n = 28) while species/morphotype-based averages for each site are shown as black dots (n = 14). Uncertainty of the lake water $\delta^{18}O$ values is site-based standard deviation among summer water samples, and uncertainty for aquatic moss samples is analytical uncertainty ($\pm 0.4\%$). For calibration curves of individual species/morphotypes of moss, see Supplementary Fig. 2 and Supplementary Fig. 3.

$$\delta^{18}O_{om}=0.635\,(\,\pm\,0.08)*\delta^{18}O_{lw}\,+\,21.24\,(\,\pm\,1.28);\,r^2=0.854;\,n=14$$
 Eq. 3

 $\alpha_{om\text{-lw}}$ for the all-species average linear regression samples is 1.0278 \pm 0.0013%.

The Species/Morphotype A only linear regression (Supplementary Fig. 2) had aquatic moss samples from seven out of the eight sites (no PL) and is given as:

$$\delta^{18}O_{om} = 0.657 \ (\pm \ 0.09) * \delta^{18}O_{lw} + 21.60 \ (\pm \ 1.46); \\ r^2 = 0.819; \ n = 14$$
 Eq. 4

 $\alpha_{om\text{-lw}}$ for the Species/Morphotype A linear regression samples is 1.0276 \pm 0.0015‰. $\delta^{18}O_{om}$ values in the Species/Morphotype A calibration samples ranged from 8.3‰ to 14.6‰.

The Species/Morphotype B only linear regression (Supplementary Fig. 3) had aquatic moss samples from five out of eight sites (LEO, PL, PWL, SPL, and NML) and is given as:

$$\delta^{18}O_{om} = 0.680\,(\pm\,0.14)*\delta^{18}O_{lw} + 21.69\,(\pm\,2.31); \\ r^2 = 0.755; \\ n = 10 \\ Eq.\, \S$$

 $\alpha_{om\text{-lw}}$ for the Species/Morphotype B linear regression samples is $1.0275\pm0.0012\%$. Species/Morphotype B had a slightly smaller range in $\delta^{18}O_{om}$ values compared to the all-species calibrations, from 8.1% to 13.9%.

To infer $\delta^{18}O_{lw}$ values from $\delta^{18}O_{om}$ values, we utilize the combined (all-species) individual strand linear regression (Fig. 6) because there are no significant differences between species/morphotypes (i.e., the uncertainty of our regression lines was greater than the differences

between the species-specific regression lines). The $\alpha_{om\text{-lw}}$ values for different species/morphotypes also fall within uncertainty of each other. This is not to say that there are no differences in using different aquatic moss species to reconstruct $\delta^{18}O_{lw}$ values, only that the differences between Greenland aquatic moss species/morphotypes in our study are smaller than our calculated uncertainties. $\delta^{18}O_{lwom}$ values ranged from -19.8 to -12.0% for the calibration samples. The standard deviation of the $\delta^{18}O_{lwom}$ values from the mean $\delta^{18}O_{lw}$ values across all sites is 1.3%. Site specific $\delta^{18}O_{lwom}$ averages were: DBL $=-17.7~\pm~1.3\%$, LEO $=-13.6~\pm~1.3\%$, NML $=-18.9~\pm~1.3\%$, PL $=-19.3~\pm~1.3\%$, PWL $=-15.5~\pm~1.3\%$, SPL $=-17.8~\pm~1.3\%$, UPL $=-17.5~\pm~1.3\%$, and WGL $=-12.4~\pm~1.3\%$. All of the site-based average $\delta^{18}O_{lwom}$ values fall

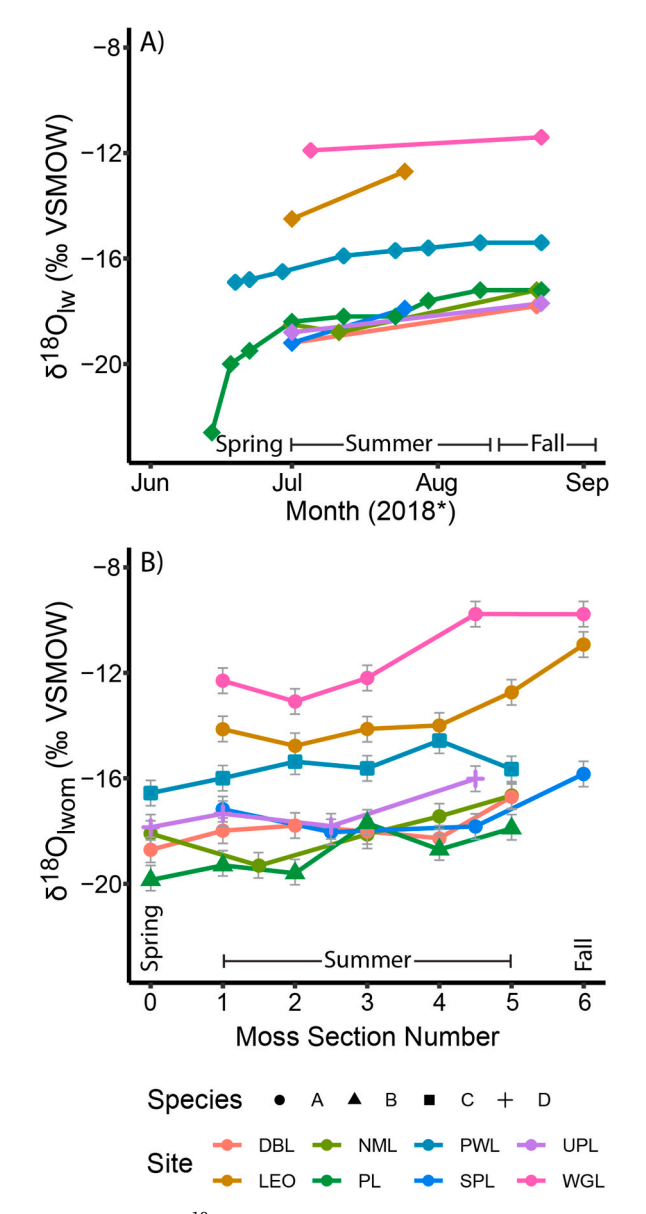


Fig. 7. A) Lake water $\delta^{18}O$ values from the eight study sites collected in 2018 (*the LEO sample is from late July 2019; Akers et al., 2023). Error associated with measurement is smaller than the size of the points. B) Lake water $\delta^{18}O$ values inferred from aquatic moss strand subsampled $\delta^{18}O$ values, using Eq. (2) derived from this study. Grey uncertainty is associated with the grey calibration regression equation in Fig. 6 ($\delta^{18}O_{lw}=1.19*\delta^{18}O_{om}-29.3; r^2=0.755; n=28; 2\sigma=\pm0.5\%$). Sites starting at 0 on the x-axis had moss strands with spring and summer seasonal growth while sites ending at 6 on the x-axis had moss strands with summer and fall growth. Spring versus fall growth were differentiated based on growth direction, and differentiated from summer growth based on overall morphology, as described in Fig. 3.

within one standard deviation of the site-based average summer $\delta^{18}O_{lw}$ measurements except WGL.

4.4. Seasonal aquatic moss δ^{18} O values

 $\delta^{18}O_{lw}$ values showed an increasing trend over July to August (Fig. 7A; Akers et al., 2023). All sites also showed an increase in summer $\delta^{18}O_{lwom}$ values from high resolution warm season aquatic moss subsamples (Fig. 7B). The magnitude of increase in $\delta^{18}O_{lw}$ values from July to August in 2018 (July 2018 to August 2019 for LEO) ranged from 0.4‰ (WGL) to 1.7‰ (LEO). The magnitude of the increase in high resolution summer $\delta^{18}O_{lwom}$ values ranged from 0.3‰ (PWL) to 2.7‰ (NML). Given the potential timing differences represented by water vs. moss samples (different years or exact seasonal timing), we do not necessarily expect the same magnitude of increase between $\delta^{18}O_{lw}$ and $\delta^{18}O_{lwom}$, but we do expect the same direction of change, as we observe (Fig. 7).

Identifying the growth direction of each warm and cold season aquatic moss strand allowed us to break each sample into either 1) spring and summer samples or 2) summer and fall samples. Seasonal specific $\delta^{18}O_{om}$ values ranged from 6.2% to 16.8% (Fig. 8A and B). Summer $\delta^{18}O_{om}$ values ranged from 6.2 to 16.0% (Fig. 8A and B). Spring $\delta^{18}O_{om}$ values ranged from 8.0 to 16.8% (Fig. 8A). Fall $\delta^{18}O_{om}$ values ranged from 9.6 to 15.7% (Fig. 8B). The average difference between consecutive summer and spring $\delta^{18}O_{om}$ values was -0.1% while the range of differences was -2.6 to 1.1% (Fig. 8C). The difference between the means of consecutive summer (n = 13) and spring (n = 13) $\delta^{18}O_{om}$ values was not statistically significant according to a one-way ANOVA (p = 0.96). The average difference between consecutive summer and fall $\delta^{18}O_{om}$ values was -1.6% while the range of differences was -3.4% to -0.2% (Fig. 8D). The difference between the means of consecutive summer (n = 11) and fall (n = 11) $\delta^{18}O_{om}$ values was not statistically significant according to a one-way ANOVA (p = 0.09).

5. Discussion

5.1. Controls on lake water δ^{18} O at Pituffik

Previous work has shown that $\delta^{18}O_{om}$ values primarily reflect $\delta^{18}O_{lw}$ values at the time of moss growth (Zhu et al., 2014; Lasher et al., 2017; Puleo et al., 2022). For our sites near Pituffik, $\delta^{18}O_{lw}$ values reflect precipitation δ¹⁸O values and, to varying degrees, enrichment of lake waters with ¹⁸O due to evaporation during the ice-free period (Akers et al., 2023). Precipitation δ^{18} O values are modified by the condensation temperature of precipitation as well as the precipitation moisture source and transportation path which vary across seasons (Dansgaard, 1964; Gat, 1996; Bowen et al., 2019). Lower local water vapor and precipitation δ^{18} O values occur in the winter season due to the lower condensation temperatures and more distant oceanic moisture sources from predominantly the Labrador Sea and north/mid Atlantic, and possibly the Pacific Northwest, as a result of greater local sea ice cover (Nusbaumer et al., 2019; Sime et al., 2019; Akers et al., 2020). The most ¹⁸O enriched precipitation falls over Pituffik in the summer months as the temperature is warmer and sea ice cover is reduced, causing moisture sourcing to shift to more local sources in Baffin Bay and the Davis Strait (Sime et al., 2019; Akers et al., 2020) with additional contributions from the Labrador Sea and terrestrial Greenland and North America (Nusbaumer et al., 2019).

The number of months of precipitation $\delta^{18}O$ values that are integrated into the waters of each lake, and the degree of evaporative enrichment, likely varies site to site due to differing residence times and whether or not the lakes experience snow melt bypass due to lake ice cover. We were able to estimate the residence time of two sites at 2.2 ± 0.4 years (LEO) and 2.3 ± 0.4 years (WGL) given the availability of lake water depth measurements. This suggests these sites contain water that has been evaporatively modified for multiple years given the higher modern $\delta^{18}O_{lw}$ values in the summer season compared to the modern

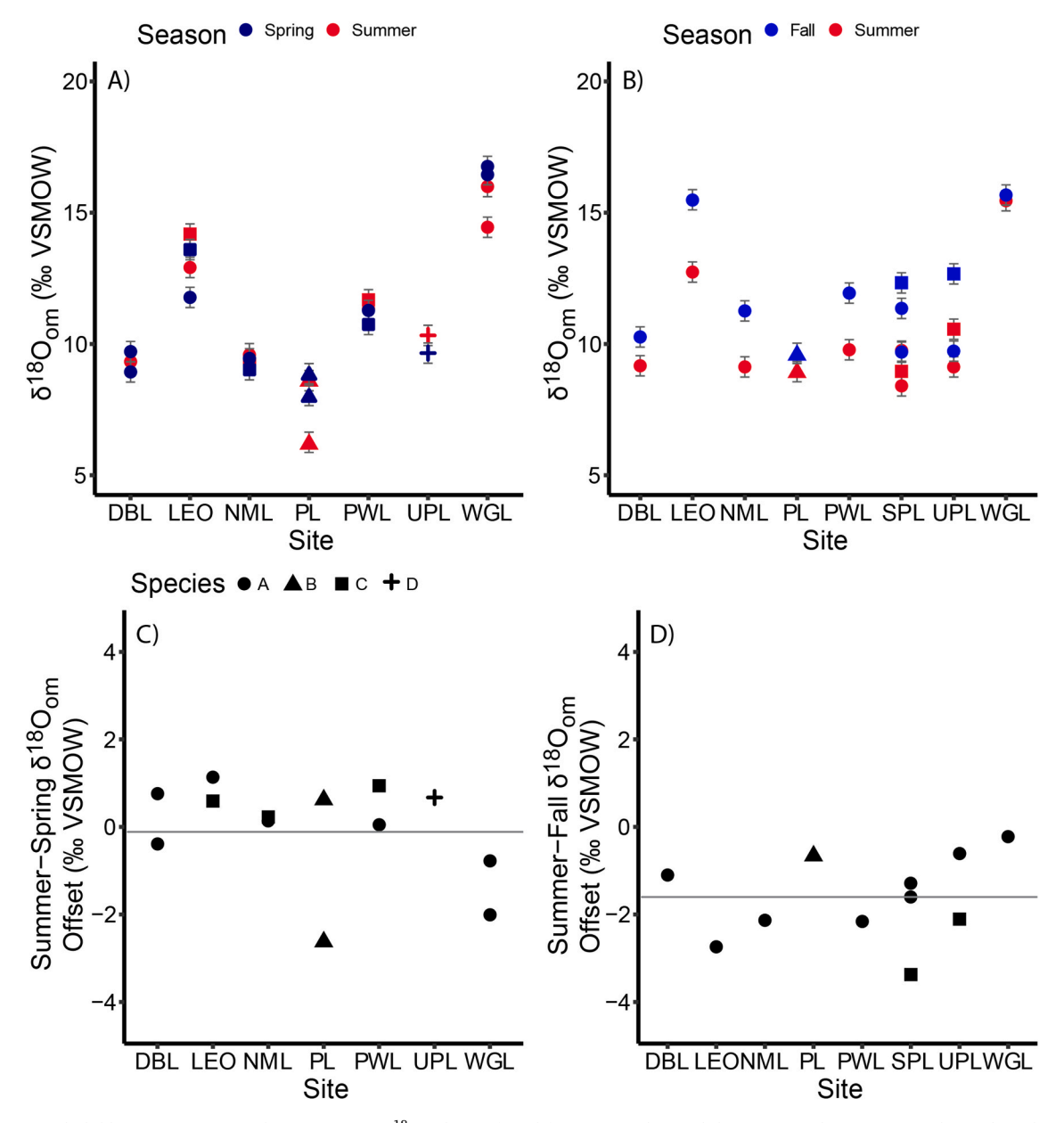


Fig. 8. A) Spring (dark blue) vs. summer (red) aquatic moss $\delta^{18}O$ values inferred from seasonal growth by site. Grey bars represent the analytical uncertainty of $\pm 0.4\%$. B) Fall (blue) vs. summer (red) aquatic moss $\delta^{18}O$ values inferred from seasonal growth segments by site. Grey bars represent the analytical uncertainty of $\pm 0.4\%$. C) Difference between summer and spring aquatic moss $\delta^{18}O$ values inferred from seasonal growth segments by site. Horizontal gray line shows mean offset. D) Difference between summer and spring aquatic moss $\delta^{18}O$ values inferred from seasonal growth segments by site. Horizontal gray line shows mean offset.

JJA weighted average precipitation $\delta^{18}O$ value (~-19.3‰). Other sites likely have shorter residence times as they have $\delta^{18}O_{lw}$ values much closer to the modern JJA weighted average precipitation $\delta^{18}O$ value (~-19.3‰) in the summer (Fig. 4A–C) and, in some cases, more depleted spring values from relatively low $\delta^{18}O$ snowpack melt input (PL; Fig. 4A). The increase in $\delta^{18}O_{lw}$ values for all sites through spring, summer, and fall is most likely driven by an increasing proportion of summer precipitation in the lakes and increased cumulative effects of evaporation, with varying degrees from site to site.

5.2. Calibrating the relationship between $\delta^{18}{\rm O}_{\rm om}$ in aquatic mosses and $\delta^{18}{\rm O}_{\rm lw}$

The linear relationships we find between $\delta^{18}O_{om}$ values and $\delta^{18}O_{lw}$ values appear reasonable, reproducible, and predictable when compared to prior calibration work between aquatic moss $\delta^{18}O$ values

and lake water δ^{18} O values in Patagonia (Zhu et al., 2014). This relationship is driven by the strong relationship between cellulose δ^{18} O values and growth water δ^{18} O values that has been demonstrated in both controlled lab conditions and in the field on Baffin Island (Sauer et al., 2001). In our study, the $\delta^{18}O_{om}$ vs. $\delta^{18}O_{lw}$ regression slope values range from 0.635 - 0.680 \pm 0.07 - 0.14 and the intercepts range from 21.24 to 21.68 ± 1.20 - 2.31 (Eqs. (2)–(5)), which differ from the slope (0.861 \pm 0.027) and intercept (27.8 \pm 0.3) determined for *Drepanocladus perpli*catus vs. growth water from Patagonia (Zhu et al., 2014). However, $\alpha_{om\text{-lw}}$ values are similar, ranging from 1.0275 to 1.0278 \pm 0.0012-0.0015 in this study compared to values of 1.0281-1.0288 derived from Drepanocladus perplicatus and water samples from Patagonia (Zhu et al., 2014). Additionally, when using $\delta^{18}O_{om}$ values to infer δ¹⁸O_{lw} values from our full calibration dataset (Fig. 6), the slope and intercept values found in this study (slope = 1.19 - 1.34; intercept = -31.0 to -29.3) compared to those found in Zhu et al., 2014 (slope = 1.16; intercept = -32.2) are very similar. We don't expect these to be identical given the differences in studied moss species, the differences in the chemical pretreatment approach, and a potential temperature dependent fractionation of cellulose (Sternberg and Ellsworth, 2011) in the very different climates.

Slight slope and intercept inconsistencies between the linear relationships presented in this study (Eqs. (2)–(5)) may result from varying percentages and isotopic compositions of major chemical compounds between moss species (Schmidt et al., 2001; Turetsky et al., 2008; Zhu et al., 2014). Another potential factor that could result in differing aquatic moss and water δ^{18} O calibration equations by species is the amount of stored carbohydrate from previous years utilized during cellulose biosynthesis, but this amount has been shown to be negligible in many aquatic mosses (Glime, 2007; Zhu et al., 2014).

Because our species/morphotype specific calibrations (Eqs. (4)–(5)) fall within uncertainty of each other, we opt to use the all species combined linear relationship for estimating δ^{18} O_{lwom} values in this study (Fig. 6). We suggest that this linear relationship can be applied to any of the studied species/morphotypes throughout the Arctic to reconstruct $\delta^{18}O_{lw}$ values from $\delta^{18}O_{om}$ values. When generating $\delta^{18}O_{lwom}$ values for paleoclimate reconstructions, we still recommend utilizing a single species as best practice given the expected differences in the chemical composition and therefore isotopic fractionation relative to growth water between different species (Schmidt et al., 2001; Turetsky et al., 2008) even though our calibrations generally fall within uncertainty of each other. This calibration may be applicable to other aquatic moss species and locations outside of the Arctic given the similarities of our observations to those presented on different species across the world (Zhu et al., 2014), but species-specific and local calibration studies are needed to achieve the greatest accuracy and confidence for reconstructing $\delta^{18}O_{lw}$ values in a given region from bulk aquatic moss strands.

5.3. Seasonal aquatic moss δ^{18} O values

Some, but not all, aquatic moss strands at our study sites had seasonally varying growth morphologies, as has been described for several species in other studies (Riis and Sand-Jensen, 1997; Li et al., 2009; Guo et al., 2013; Riis et al., 2014; Thiemer et al., 2018; Xia et al., 2020). We assume that spring growth reflects mid to late June $\delta^{18}O_{lw}$ values, summer growth reflects July to mid-August $\delta^{18} O_{lw}$ values, and fall growth reflects late August to early September $\delta^{18}O_{lw}$ values. Mid to late June is the period of initial lake ice moating (and for small, shallow ponds, complete loss of lake ice), July to mid-August is when lake ice cover is completely gone, and late August to early September is the typical period of lake ice growth before complete ice cover reestablishes. These seasons have above freezing bottom water temperatures and sufficient light availability for moss growth. Some moss species can grow under complete ice cover (Rankin et al., 2017); however, we suspect the majority of growth occurs after ice cover thins in spring and before complete ice cover establishes in fall. We argue that no growth occurs from early November to middle February due to polar night at this latitude and the absence of light for photosynthesis (Glime, 2007).

Summer growth segments sectioned into a high-resolution time series of $\delta^{18}O_{om}$ values successfully record $\delta^{18}O_{lw}$ values at biweekly to monthly resolution. $\delta^{18}O_{lwom}$ values from a single subsampled summer aquatic moss strand generally increase comparably to summer 2018 $\delta^{18}O_{lw}$ values from our eight sites (Fig. 7A and B; Akers et al., 2023). This increasing trend appears in all sites regardless of lake water residence time. The magnitude of change in $\delta^{18}O_{lw}$ values over July and August is similar to the $\delta^{18}O_{lwom}$ changes across a single summer season at sites DBL, LEO, PL, SPL, and UPL. Assuming summer $\delta^{18}O_{lw}$ values and summer $\delta^{18}O_{lwom}$ values should shift by the same amount, it appears most summer-morphology ("bushy") moss growth indeed occurred in July and August at these sites. Larger differences between summer shifts in $\delta^{18}O_{lwom}$ values and $\delta^{18}O_{lw}$ values exist at sites NML, PWL, and WGL. We hypothesize that for these sites, the temporal resolution of the

sampling of the aquatic moss strands and the waters differed as a result of the moss strands growing in a different year and/or over a different duration of the summer.

Sectioning of mosses into spring, summer, and fall growth provides additional encouraging results regarding the potential for seasonal reconstructions of $\delta^{18}O_{lw}$ values. Spring and summer $\delta^{18}O_{om}$ values are quite similar on average ($\sim 0.1\%$ offset; p = 0.96; Fig. 8C) while fall $\delta^{18}O_{om}$ values are higher on average than summer $\delta^{18}O_{om}$ values (\sim 1.6% offset; p = 0.09; Fig. 8D). The minimal offset between spring and summer $\delta^{18}O_{om}$ values could be attributable to a lagged late summer signal that gets trapped when it freezes over during the previous winter, isotopically light spring melt partially bypassing some of the lakes due to ice cover, lower rates of evaporation in the spring and early summer, and/or a smaller portion of the lake volume filled with ¹⁸O enriched summer precipitation in early summer. Additionally, the similarity of spring and summer $\delta^{18}O_{om}$ values could suggest that summer growth segments we sampled for seasonal comparison grew mostly in the early summer (when $\delta^{18}O_{lw}$ values were most similar to $\delta^{18}O_{lw}$ values in spring), unlike our summer subsampled strands which grew throughout the summer. Enrichment of $\delta^{18}O_{om}$ values in the fall is expected due to the cumulative evaporative effects throughout the ice-free season and the relative dominance of ¹⁸O enriched summer precipitation at the end of summer. Although there are far more leaves on summer moss subsamples compared to spring or fall ones, we do not suspect that differences in $\delta^{18} O_{om}$ values in stem vs. leaf tissue would result in a substantial difference in our seasonal $\delta^{18}O_{om}$ values given the similarity of $\delta^{18}O_{om}$ values found in Drepanocladus stems vs. leaves from Patagonia (Zhu et al., 2014).

Temperature dependent fractionations could potentially have significant effects on observed isotopic differences between spring, summer, and fall moss segments at these sites given the region's large seasonal temperature shifts, but quantifying the magnitude of a potential temperature-dependent fractionation effect occurring during cellulose biosynthesis remains uncertain (DeNiro and Epstein, 1981; Sternberg and Ellsworth, 2011; Zech et al., 2014; Zhu et al., 2014; Mayr et al., 2015; Hirl et al., 2021; Xia and Yu, 2020). Cellulose is a major chemical constituent of aquatic mosses (40-60%; Turetsky et al., 2008) and source of oxygen to our $\delta^{18}O_{om}$ measurements. However, Sternberg and Ellsworth (2011) suggest that the fractionation of cellulose δ^{18} O relative to growth water δ^{18} O varies significantly at lower temperatures. Following their results, the approximate range of lake water temperatures at Pituffik (based on data from Wax Lips Lake 60 km northeast of Pituffik) would produce fractionation variability from 30.5% at 5 °C to 28.9‰ at 10 °C. This potential temperature-dependent fractionation effect would cause our spring and summer $\delta^{18}O_{om}$ values to be more similar due to the larger fractionation factor in the cooler spring compared to the smaller fractionation factor in the warmer summer. Therefore, even if spring $\delta^{18}O_{lw}$ values were lower than summer $\delta^{18}O_{lw}$ values as we observe in our lakes, it may not be reflected by our $\delta^{18}O_{om}$ values because the changing fractionation factors would work in the opposite direction.

Future studies comparing bulk aquatic moss $\delta^{18}O$ values and cellulose $\delta^{18}O$ values of several aquatic moss species with growth water $\delta^{18}O$ values at known temperatures ranging from 1 to 20 °C under controlled lab or well-constrained field conditions are needed to constrain potential temperature-dependent fractionation effects. Still, there is no current literature consensus on the degree of temperature-dependent fractionations in cellulose biosynthesis. Additionally, the influence of a temperature-dependent fractionation effect on bulk moss $\delta^{18}O$ values (rather than pure cellulose) has not yet been explored. Due to this uncertainty, we do not attempt to reconstruct $\delta^{18}O_{lwom}$ from the spring/summer/fall time series of moss growth or apply a temperature correction factor to our reconstructions at this time.

6. Conclusion

Overall, we find robust evidence that $\delta^{18}O$ values of submerged aquatic moss strands from Greenland reflect lake water $\delta^{18}\text{O}$ values, and that progressive moss growth from spring to fall preserves a record of seasonal shifts in lake water δ^{18} O values. Oxygen isotope values of short segments of aquatic moss strands can reflect the evolution of lake water δ^{18} O values on a weekly to monthly scale through the growing season. Summer and fall seasonal moss strand $\delta^{18}\text{O}$ values record summer-to-fall shifts in lake water $\delta^{18}\text{O}$ values attributable to cumulative inputs of ^{18}O enriched summer precipitation and evaporative modification through late summer and fall. This provides precedent for creating highresolution reconstructions of seasonal lake water $\delta^{18}O$ values back in time. Where subfossil aquatic brown mosses are preserved well enough to distinguish seasons of growth, seasonally resolved lake water δ^{18} O reconstructions are possible. Even in cases where aquatic moss seasonal growth morphology is not well preserved, overall variability of lake water δ^{18} O throughout the growing season could be assessed by measuring δ^{18} O values of continuous subsamples along moss strands. The seasonal variability captured by growing mosses means that researchers using mosses and paleo-archives of lake water δ^{18} O values should carefully consider whether to subsample single strands to achieve a high temporal resolution or homogenize multiple strands to reconstruct average conditions. Between-species differences in biosynthetic fractionations were insignificant among the species/morphotypes we analyzed, and our study finds similar fractionation factors (α_{om-lw} = \sim 1.0278 \pm 0.0014) to those reported previously ($\alpha_{om\text{-lw}} = \sim$ 1.0285 \pm 0.0003).

To continue to develop this method into a valuable paleoclimate proxy, further work is needed. This includes:

- 1) Developing additional $\delta^{18}O_{om}$ vs. $\delta^{18}O_{lw}$ calibration studies globally and with a variety of aquatic moss species.
- 2) Determining the effects of chemical pretreatment on the oxygen isotope fractionation of aquatic mosses relative to host water.
- 3) Quantifying the presence and extent of any temperature-dependent fractionation effects in bulk aquatic moss and moss cellulose at low temperatures with controlled lab experiments or well constrained field samples.
- 4) Investigating the preservation of aquatic moss seasonal growth morphologies back in time in sediment cores.
- Deploying measurements of continuously subsampled aquatic moss strands sampled from sediment cores back in time.

CRediT authorship contribution statement

Peter J.K. Puleo: Conceptualization, Methodology, Formal analysis, Investigation, Data curation, Writing – original draft, Writing – review & editing, Visualization, Project administration, Funding acquisition. Pete D. Akers: Data curation, Writing – review & editing, Project administration, Funding acquisition. Ben G. Kopec: Data curation, Writing – review & editing, Project administration, Funding acquisition. Hannah Bailey: Data curation, Writing – review & editing, Project administration, Funding acquisition. Hannah Bailey: Data curation, Writing – review & editing, Project administration, Funding acquisition. Tenna Riis: Writing – review & editing. Yarrow Axford: Conceptualization, Methodology, Formal analysis, Resources, Data curation, Writing – review & editing, Visualization, Supervision, Project administration, Funding acquisition.

Declaration of competing interest

The authors declare that they have no known competing financial interests or personal relationships that could have appeared to influence the work reported in this paper.

Data availability

Data is available at the NSF Arctic Data Center (https://arcticdata.io/).

Acknowledgements

We thank the people of Kalaallit Nunaat, known in English as Greenland, for granting researchers access to their lands. We thank Jamie McFarlin for helpful discussions of isotope effects, Jennifer Burnham for insights about when to conduct sampling, Aino Erkinaro for assistance with water isotope analysis, and Mia Tuccillo, Sarah Scott, Kevin Myers, Kurt Burnham and the High Arctic Institute, Anna Zajicek and Polar Field Services, U.S. Air Mobility Command and the personnel of Pituffik Space Base (which at the time of field work was known as Thule Air Base) for assistance and support during fieldwork. This work was supported by NSF Office of Polar Programs award to Axford and Osburn [grant number 2002515]. It was also financially supported by NSF Office of Polar Programs [grant numbers 1504141 and 1852614] and by the Inaugural UArctic Research Chairship to Welker. Bailey is supported by the Research Council of Finland [grant number 348536].

Appendix A. Supplementary data

Supplementary data to this article can be found online at https://doi.org/10.1016/j.quascirev.2024.108682.

References

- Akers, P.D., Kopec, B.G., Mattingly, K.S., Klein, E.S., Causey, D., Welker, J.M., 2020. Baffin Bay sea ice extent and synoptic moisture transport drive water vapor isotope $(\delta^{18} \text{O}, \, \delta^2 \text{H}, \, \text{and deuterium excess})$, and deuterium excess) variability in coastal northwest Greenland. Atmos. Chem. Phys. 20, 13929–13955.
- Akers, P.D., Kopec, B.G., Klein, E.S., Welker, J.M., 2023. Evaporation and water sourcing dominate lake and stream isotopic variability across time and space in a High Arctic periglacial landscape. ESS Open Archive 1–58. https://doi.org/10.22541/ essoar.169444333.36870371/v1.
- Allen, S.T., Jasechko, S., Berghuijs, W.R., Welker, J.M., Goldsmith, G.R., Kirchner, J.W., 2019. Global sinusoidal seasonality in precipitation isotopes. Hydrol. Earth Syst. Sci. 23, 3423–3436.
- Alley, R., 2000. The Younger Dryas cold interval as viewed from central Greenland. Quat. Sci. Rev. 19, 213–226.
- Alley, R., Ágústsdóttir, A., 2005. The 8k event: cause and consequences of a major Holocene abrupt climate change. Quat. Sci. Rev. 24, 1123–1149.
- Axford, Y., De Vernal, A., Osterberg, E.C., 2021. Past warmth and its impacts during the Holocene thermal maximum in Greenland. Annu. Rev. Earth Planet. 49, 279–307.
- Bowen, G.J., 2023. The online isotopes in precipitation calculator version 3.1. http://www.waterisotopes.org.
- Bowen, G.J., Cai, Z., Fiorella, R.P., Putman, A.L., 2019. Isotopes in the water cycle: regional- to global-scale patterns and applications. Annu. Rev. Earth Planet. 47, 453–479.
- Bowen, G.J., Wassenaar, L.I., Hobson, K.A., 2005. Global application of stable hydrogen and oxygen isotopes to wildlife forensics. Oecologia 143, 337–348.
- Buizert, C., Keisling, B.A., Box, J.E., He, F., Carlson, A.E., Sinclair, G., DeConto, R.M., 2018. Greenland-Wide Seasonal Temperatures During the Last Deglaciation. Geophysical Research Letters 45, 1905–1914.
- Cappelen, J., Drost Jensen, C., 2021. Climatological Standard Normals 1991-2020 Greenland the Climate of Greenland - with Climatological Standard Normals, 1991-2020. Report 21-12, DMI, Copenhagen.
- Collins, C.G., Elmendorf, S.C., Hollister, R.D., Henry, G.H.R., Clark, K., Bjorkman, A.D., Myers-Smith, I.H., Prevey, J.S., Ashton, I.W., Assmann, J.J., Alatalo, J.M., Carbognani, M., Chisholm, C., Cooper, E.J., Forrester, C., Jonsdottir, I.S., Klanderud, K., Kopp, C.W., Livensperger, C., Mauritz, M., May, J.L., Molau, U., Oberbauer, S.F., Ogburn, E., Panchen, Z.A., Petraglia, A., Post, E., Rixen, C., Rodenhizer, H., Schuur, E.A.G., Semenchuk, P., Smith, J.G., Steltzer, H., Totland, O., Walker, M.D., Welker, J.M., Suding, K.N., 2021. Experimental warming differentially affects vegetative and reproductive phenology of tundra plants. Nat. Commun. 12, 3442.
- Corbett, L.B., Bierman, P.R., Lasher, G.E., Rood, D.H., 2015. Landscape chronology and glacial history in Thule, northwest Greenland. Quat. Sci. Rev. 109, 57–67.
- Corcoran, M.C., Thomas, E.K., Morrill, C., 2021. Using a paired chironomid δ^{18} O and aquatic leaf wax δ^{2} H approach to reconstruct seasonality on western Greenland during the Holocene. Paleoceanogr. Paleoclimatol. 36, 1–18.
- Dansgaard, W., 1964. Stable isotopes in precipitation. Tellus 16, 436–468.
- Dawes, P.R., 1975. Reconnaissance of the Thule group and underlying basement rocks between inglefield bredning and Melville Bugt, western north Greenland. Rapp. Grønl. Nor. Geol. Unders. 75, 34–38.

- Dawes, P.R., Rex, D.C., Jepsen, H.F., 1973. K/Ar whole rock ages of dolerites from the Thule district, western north Greenland. Rapp. Grønl. Geol. Unders. 55, 61–66.
- DeNiro, M.J., Epstein, S., 1981. Isotopic composition of cellulose from aquatic organisms. Geochem. Cosmochim. Acta 45, 1885–1894.
- Denton, G., Alley, R., Comer, G., Broecker, W., 2005. The role of seasonality in abrupt climate change. Quat. Sci. Rev. 24, 1159–1182.
- Fastovich, D., Russell, J.M., Jackson, S.T., Williams, J.W., 2020. Deglacial temperature controls on no-analog community establishment in the Great Lakes Region. Quat. Sci. Rev. 234.
- Fréchette, B., de Vernal, A., Guiot, J., Wolfe, A.P., Miller, G.H., Fredskild, B., Kerwin, M. W., Richard, P.J.H., 2008. Methodological basis for quantitative reconstruction of air temperature and sunshine from pollen assemblages in Arctic Canada and Greenland. Quat. Sci. Rev. 27, 1197–1216.
- Gat, J.R., 1996. Oxygen and hydrogen isotopes in the hydrologic cycle. Annu. Rev. Earth Planet. 24, 225–262.
- Glime, J.M., 2007. Bryophyte Ecology Volume 1: Physiological Ecology. Michigan Technological University and the International Association of Bryologists. http://www.bryoecol.mtu.edu.
- Greene, C.A., Gardner, A.S., Wood, M., Cuzzone, J.K., 2024. Ubiquitous acceleration in Greenland ice Sheet calving from 1985 to 2022. Nature 625, 523–528.
- Guo, C.-Q., Ochyra, R., Wu, P.-C., Seppelt, R.D., Yao, Y.-F., Bian, L.-G., Li, S.-P., Li, C.-S., 2013. Warnstorfia exannulata, an aquatic moss in the Arctic: seasonal growth responses. Clim. Change 119, 407–419.
- Harning, D., Raberg, J., McFarlin, J., Axford, Y., Florian, C., Ólafsdóttir, K., Kopf, S., Sepúlveda, J., Miller, G., Geirsdóttir, Á., 2024. Spatiotemporal variation of modern lake, stream, and soil water isotopes in Iceland. Hydrol. Earth Syst. Sci. 1–35. https://doi.org/10.5194/hess-2024-1.
- Hedenäs, L., Bennike, O., 2003. Moss remains from the last interglacial at Thule, NW Greenland. Lindbergia 28, 52–58.
- Hirl, R.T., Ogee, J., Ostler, U., Schaufele, R., Baca Cabrera, J.C., Zhu, J., Schleip, I., Wingate, L., Schnyder, H., 2021. Temperature-sensitive biochemical ¹⁸Ofractionation and humidity-dependent attenuation factor are needed to predict delta ¹⁸O of cellulose from leaf water in a grassland ecosystem. New Phytol. 229, 3156–3171.
- Holland, K.M., Porter, T.J., Froese, D.G., Kokelj, S.V., Buchanan, C.A., 2020. Ice-wedge evidence of Holocene winter warming in the Canadian arctic. Geophys. Res. Lett. 47, 1–10
- IAEA/WMO, 2015. Global Network of isotopes in precipitation, GNIP database. Accessible at: https://nucleus.iaea.org/wiser.
- Lasher, G.E., Axford, Y., McFarlin, J.M., Kelly, M.A., Osterberg, E.C., Berkelhammer, M. B., 2017. Holocene temperatures and isotopes of precipitation in Northwest Greenland recorded in lacustrine organic materials. Quat. Sci. Rev. 170, 45–55.
- Li, S.-P., Ochyra, R., Wu, P.-C., Seppelt, R.D., Cai, M.-H., Wang, H.-Y., Li, C.-S., 2009. Drepanocladus longifolius (Amblystegiaceae), an addition to the moss flora of king George Island, south Shetland Islands, with a review of Antarctic benthic mosses. Polar Biol. 32, 1415–1425.
- Longo, W.M., Huang, Y., Russell, J.M., Morrill, C., Daniels, W.C., Giblin, A.E., Crowther, J., 2020. Insolation and greenhouse gases drove Holocene winter and spring warming in Arctic Alaska. Quat. Sci. Rev. 242.
- Manolaki, P., Pastor, A., Karttunen, K., Guo, K., Riis, T., 2022. Effects of temperature and nutrient enrichment on the Arctic moss Hygrohypnella ochracea growth and productivity. Polar Biol. 45, 1415–1425.
- Marcott, S.A., Shakun, J.D., Clark, P.U., Mix, A.C., 2013. A reconstruction of regional and global temperature for the past 11,300 years. Science 339, 1198–1201.
- Mayr, C., Laprida, C., Lücke, A., Martín, R.S., Massaferro, J., Ramón-Mercau, J., Wissel, H., 2015. Oxygen isotope ratios of chironomids, aquatic macrophytes and ostracods for lake-water isotopic reconstructions – results of a calibration study in Patagonia. J. Hydrol. 529, 600–607.
- McFarlin, J.M., Axford, Y., Kusch, S., Masterson, A.L., Lasher, G.E., Osburn, M.R., 2023. Aquatic plant wax hydrogen and carbon isotopes in Greenland lakes record shifts in methane cycling during past Holocene warming. Sci. Adv. 9 https://doi.org/ 10.1126/sciadv.adh9704.
- McFarlin, J.M., Axford, Y., Osburn, M.R., Kelly, M.A., Osterberg, E.C., Farnsworth, L.B., 2018. Pronounced summer warming in northwestnorthwest Greenland during the Holocene and last interglacial. Proc. Natl. Acad. Sci. U.S.A. 115, 6357–6362, 2018.
- Meyer, H., Opel, T., Laepple, T., Dereviagin, A.Y., Hoffmann, K., Werner, M., 2015. Long-term winter warming trend in the Siberian Arctic during the mid- to late Holocene. Nat. Geosci. 8, 122–125.
- Nusbaumer, J., Alexander, P.M., LeGrande, A.N., Tedesco, M., 2019. Spatial shift of Greenland moisture sources related to enhanced arctic warming. Geophys. Res. Lett. 46 (14,723–714), 731.

- Porter, C., Morin, P., Howat, I., Noh, M.J., Bates, B., Peterman, K., Keesey, S., Schlenk, M., Gardiner, J., Tomko, K., Willis, M., Kelleher, C., Cloutier, M., Husby, E., Foga, S., Nakamura, H., Platson, M., Wethington, M., Williamson, C., Bauer, G., Enos, J., Arnold, G., Kramer, W., Becker, P., Doshi, A., D'Souza, C., Cummens, P., Laurier, F., Bojesen, M., 2018. ArcticDEM, Harvard Dataverse V1. https://doi.org/10.7910/DVN/OHHUKH.
- Puleo, P.J.K., Masterson, A.L., Medeiros, A.S., Schellinger, G., Steigleder, R., Woodroffe, S., Osburn, M.R., Axford, Y., 2022. Younger Dryas and early Holocene climate in south Greenland inferred from oxygen isotopes of chironomids, aquatic Moss, and Moss cellulose. Quat. Sci. Rev. 296, 1–16.
- Rankin, A.H., Pressel, S., Duckett, J., Rimington, W.R., Hawes, I., Sumner, D.Y., Mackey, T.J., Castendyke, D., Schneider, H., Jungblut, A.D., 2017. Characterization of a deep-water moss from the perennially ice-covered Lake Vanda, Antarctica. Polar Biol. 40, 2063–2076.
- Richter, N., Russell, J.M., Garfinkel, J., Huang, Y., 2021. Winter–spring warming in the North Atlantic during the last 2000 years: evidence from southwest Iceland. Clim. Past 17, 1363–1383.
- Riis, T., Christoffersen, K.S., Baattrup-Pedersen, A., 2014. Effects of warming on annual production and nutrient-use efficiency of aquatic mosses in a high Arctic lake. Freshw. Biol. 59, 1622–1632.
- Riis, T., Olesen, B., Katborg, C.K., Christoffersen, K.S., 2010. Growth rate of an aquatic bryophyte (Warnstorfia fluitans (Hedw.) Loeske) from a high Arctic lake: effect of nutrient concentration. Arctic 63, 100–106.
- Riis, T., Sand-Jensen, K., 1997. Growth reconstruction and photosynthesis of aquatic mosses: influence of light, temperature and carbon dioxide at depth. J. Ecol. 85, 359–372
- Sand-Jensen, K., Riis, T., Markager, S., Vincent, W.F., 1999. Slow growth and decomposition of mosses in Arctic lakes. Can. J. Fish. Aquat. Sci. 56, 388–393.
- Sauer, P.E., Miller, G.H., Overpeck, J.T., 2001. Oxygen isotope ratios of organic matter in arctic lakes as a paleoclimate proxy: field and laboratory investigations. J. Paleolimnol. 25, 43–64.
- Schmidt, H.L., Werner, R.A., Roßmann, A., 2001. ¹⁸O Pattern and biosynthesis of natural plant products. Phytochemistry (Elsevier) 58, 9–32.
- Seppä, H., Birks, H.J.B., Odland, A., Poska, A., Veski, S., 2004. A modern pollen-climate calibration set from northern Europe: developing and testing a tool for palaeoclimatological reconstructions. J. Biogeogr. 31, 251–267.
- Sime, L.C., Hopcroft, P.O., Rhodes, R.H., 2019. Impact of abrupt sea ice loss on Greenland water isotopes during the last glacial period. Proc. Natl. Acad. Sci. USA 116, 4099–4104.
- Steere, W.C., 1975. Mosses and hepatics from the Thule district, northwestern Greenland. Am. Midl. Nat. 94, 326–347.
- Steere, W.C., 1939. Bryophyta of arctic America, II. Am. Midl. Nat. 21, 355-367.
- Sternberg, L., Ellsworth, P.F., 2011. Divergent biochemical fractionation, not convergent temperature, explains cellulose oxygen isotope enrichment across latitudes. PLoS One 6, 1–7. https://doi.org/10.1371/journal.pone.0028040.
- Thiemer, K., Christiansen, D.M., Petersen, N.S., Mortensen, S.M., Christofersen, K.S., 2018. Reconstruction of annual growth in relation to summer temperatures and translocation of nutrients in the aquatic moss Drepanocladus trifarius from West Greenland. Polar Biol. 41, 2311–2321.
- Thomas, E.K., Hollister, K.V., Cluett, A.A., Corcoran, M.C., 2020. Reconstructing arctic precipitation seasonality using aquatic leaf wax δ^2 H in lakes with contrasting residence times. Paleoceanogr. Paleoclimatol. 35, 1–19.
- Turetsky, M.R., Crow, S.E., Evans, R.J., Vitt, D.H., Wieder, R.K., 2008. Trade-offs in resource allocation among moss species control decomposition in boreal peatlands. J. Ecol. 96, 1297–1305.
- Verbruggen, F., Heiri, O., Reichart, G.J., De Leeuw, J.W., Nierop, K.G.J., Lotter, A.F., 2010. Effects of chemical pretreatments on δ¹⁸O measurements, chemical composition, and morphology of chironomid head capsules. J. Paleolimnol. 43, 857–872.
- Xia, Z., Yu, Z., 2020. Temperature-dependent oxygen isotope fractionation in plant cellulose biosynthesis revealed by a global dataset of peat mosses. Front. Earth Sci. 8, 1–13.
- Xia, Z., Zheng, Y., Stelling, J.M., Loisel, J., Huang, Y., Yu, Z., 2020. Environmental controls on the carbon and water (H and O) isotopes in peatland Sphagnum mosses. Geochem. Cosmochim. Acta 277, 265–284.
- Zech, M., Mayr, C., Tuthorn, M., Leiber-Sauheitl, K., Glaser, B., 2014. Oxygen isotope ratios (¹⁸O/¹⁶O) of hemicellulose-derived sugar biomarkers in plants, soils and sediments as paleoclimate proxy I: insight from a climate chamber experiment. Geochem. Cosmochim. Acta 126, 614–623.
- Zhu, J., Lücke, A., Wissel, H., Mayr, C., Ohlendorf, C., Zolitschka, B., 2014. Characterizing oxygen isotope variability and host water relation of modern and subfossil aquatic mosses. Geochem. Cosmochim. Acta 130, 212–228.